This is an *Accepted Manuscript*, which has been through the RSC Publishing peer review process and has been accepted for publication.

Accepted Manuscripts are published online shortly after acceptance, which is prior to technical editing, formatting and proof reading. This free service from RSC Publishing allows authors to make their results available to the community, in citable form, before publication of the edited article. This *Accepted Manuscript* will be replaced by the edited and formatted *Advance Article* as soon as this is available.

To cite this manuscript please use its permanent Digital Object Identifier (DOI®), which is identical for all formats of publication.

More information about *Accepted Manuscripts* can be found in the **Information for Authors**.

Please note that technical editing may introduce minor changes to the text and/or graphics contained in the manuscript submitted by the author(s) which may alter content, and that the standard **Terms & Conditions** and the **ethical guidelines** that apply to the journal are still applicable. In no event shall the RSC be held responsible for any errors or omissions in these *Accepted Manuscript* manuscripts or any consequences arising from the use of any information contained in them.

Carbon Nanotube-Supported Dendritic Pt-on-Pd Nanostructures: Growth Mechanism and Electrocatalytic Activity Towards Oxygen Reduction

Sourov Ghosh, Siniya Mondal and C. Retna Raj*

Department of Chemistry, Indian Institute of Technology Kharagpur

Kharagpur 721302, India

E-mail: crraj@chem.iitkgp.ernet.in
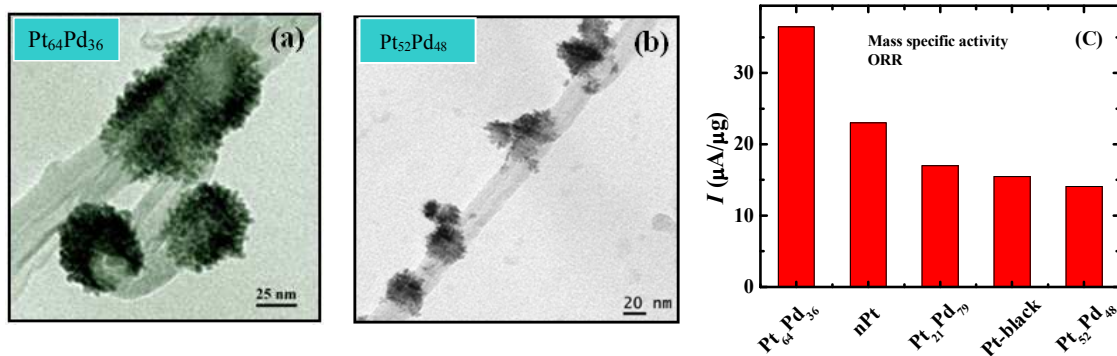
Abstract

We describe the growth of Pt-on-Pd dendritic nanostructures of different compositions ($Pt_{64}Pd_{36}$, $Pt_{52}Pd_{48}$ and $Pt_{21}Pd_{79}$) over multiwall carbon nanotubes (MWCNTs) and the electrocatalytic performance towards oxygen reduction reaction (ORR). The reduction of metal precursors ($PtCl_6^{2-}$ and $PdCl_4^{2-}$) was achieved using ascorbic acid (AA) in the absence of surfactants or shape regulating agents. The difference in the reduction potential of Pt and Pd precursors favors their sequential reduction. The mechanism for the growth of dendritic nanostructure involves (i) the initial reduction of Pd(II) and Pt(IV) complexes to Pd(0) and Pt(II), (ii) complexation of in situ generated dehydroascorbic acid (DHA), with Pt(II) species, (iii) reduction of Pt(II)-DHA complex by the excess AA and the growth of dendritic nanostructure over the surface-confined Pd seeds. The bimetallic nanostructures have 25-55 nm size with an average branch width of 2-3 nm. Elemental composition-dependent electrocatalytic performance of the bimetallic nanostructures towards ORR was evaluated in terms of specific activity, onset potential and durability. The nanoelectrocatalyst of $Pt_{64}Pd_{36}$ composition has the highest area and mass specific activity at 0.9 V (342 $\mu A/cm^2$, 36.5 $\mu A/\mu g$) and is highly durable compared to other compositions. Electrocatalytic activity of the bimetallic nanoelectrocatalyst is compared with conventional spherical nanoparticles synthesized at identical condition as well as with the commercial catalyst. The area specific activity of $Pt_{64}Pd_{36}$ composition was found to be ~7.5 times higher than the commercial Pt black, reflecting its superior electrocatalytic activity.

Introduction

The electroreduction of oxygen is of great interest owing to its important role as the rate-determining reaction in corrosion processes and electrochemical energy conversion devices such as fuel cells.[1-3] Pt has been traditionally used as catalyst for oxygen reduction reaction (ORR). It is known that the sluggish electron transfer kinetics on Pt electrocatalyst leads to high overpotential and very low efficiency in fuel cell.[4] The Pt-based alloy and core-shell nanostructures exhibit high catalytic activity compared to the conventional Pt catalyst.[5-11] For instance, enhancement in the catalytic activity towards ORR by a factor of 1.5 to 3 has been achieved with the bimetallic nanostructures.[8-10] The enhancement in the catalytic activity has been ascribed to composition, shape, size, crystallographic orientation, etc. The structural and electronic effects contribute to the enhancement in the catalytic activity. The d-band vacancy of metal catalyst is known to have profound effect in the catalytic activity of the nanoparticles towards ORR.[12] Nørskov's group introduced a theoretical model rationalizing the catalytic activity of metals with d-band structure.[13-16] The adsorption of oxygen on catalyst surface depends upon the extent of d-band vacancy of metals; metal with d-band vacancy of 0.6 per atom can favor the adsorption of oxygen neither too weak nor too strong.[12] Shao $et\ al$. reported that Pd overlayer electrocatalyst on Pd-Fe alloy shows high electrocatalytic activity due to successful manipulation of d-band energy with optimal adsorption energy for O_2 as well as facilitated removal of adsorbed hydroxyl ions.[17] Zhou $et\ al$. demonstrated the enhanced electrocatalytic activity of segregated Pd layer over $Pd_3Fe(111)$ annealed surface.[18] The segregated Pd layer has a similar ORR activity as Pt(111) due to downshift of d-band centre, but has poor stability due to dissolution of subsurface Fe in acidic environment. To enhance the stability, the catalyst was further modified with Pt-monolayer (Pt_{ML}) and the electrocatalytic activity of Pt_{ML}/Pd/annealed-

Pd$_3$Fe(111) was found to show higher activity than Pt$_{ML}$/Pd(111) because of further downshift of d-band centre which facilitates weakening of Pt-OH bond.[18] Strasser *et al*. demonstrated the electrocatalytic activity of dealloyed Pt-Cu core shell nanoparticles toward ORR by considering the lattice strain at Pt-shell of alloy core, which modify the d-band structure of Pt-atoms and weakens the adsorption energy of reactive intermediate of ORR.[19] Kitchin*et al*. demonstrated that a subsurface of $3d$ metal layer can effectively manipulate the d-band structure of Pt surface and thereby weakens the dissociative adsorption energy of hydrogen/oxygen.[14]Among the various bimetallic nanoelectrocatalyst, the Pt-Pd bimetallic nanoparticles are very promising and demonstrated to be an efficient electrocatalyst for ORR.[20-25] The choice of Pt and Pd for the synthesis of bimetallic electrocatalyst is to integrate the merits of both the metals toward oxygen reduction. Due to the similar unit cell structure of Pt and Pd, epitaxial growth can be observed in the Pt-Pd bimetallic nanostructures through the atomic level manipulation of physical and electronic properties, which is being manifested in their electrocatalytic performances. Recently, Adzic's group has reported the electrocatalytic activity of Pt thin layer on Pd nanowire as efficient electrocatalyst for oxygen reduction.[20] The high electrocatalytic activity was attributed to the under-layered Pd induced contraction of Pt surface, which weakens the OH adsorption and thereby increases ORR activity.

Several methodologies have been adopted for the synthesis of ORR active bimetallic nanostructures. The galvanic displacement reaction, polyol, seed-mediated and surfactant-assisted methods are widely used.[26-28] Ascorbic acid (AA) has been extensively used as a reducing agent in the surfactant-assisted and seed-mediated methods for the synthesis of bimetallic Pt-Pd nanostructures.[28-32,33,34] For instance, Yamauchi's group synthesized Pt and Pt-Pd nanoparticles in surfactant solution using AA as a reducing agent.[30-32] On the other hand,

Xia's group pioneered the seed-mediated growth approach for the synthesis of Pt-Pd bimetallic nanostructure using poly(vinyl pyrrolidone) and AA.[24,35,36] Zhang's group employed the surfactant-assisted microwave method using AA as a reducing agent.[33] Surfactant or polymer has been used as a structure regulating reagent in all these synthetic protocols. Our group is interested in the synthesize of catalytically active mono and bimetallic nanostructures for fuel cell reactions.[25,37-40] In an attempt to synthesis active bimetallic nanostructure, herein we describe facile room temperature synthesis of MWCNT-supported dendritic Pt-on-Pd catalyst and their electrocatalytic performance. The nanoparticles were synthesized using mild reducing agent AA without any surfactant. The aim of this study is to (i) explore the actual mechanism of the reduction of Pt(IV) and Pd(II) precursors in the absence of surfactants or polymers and (ii) exploit the bimetallic nanostructures for the electrocatalytic reduction of oxygen. To understand the effect of composition, Pt/Pd atomic ratio has been varied and ORR activity of the resulting electrocatalysts has been tested. The catalytic performance of the bimetallic nanostructures was compared with the commercial Pt catalyst.

Experimental Section

Materials: $H_2PtCl_6.6H_2O$, K_2PdCl_4, MWCNTs were obtained from Sigma-Aldrich. AA was purchased from Sisco research laboratory (India). MWCNTs were used after purification using standard literature procedures. All other chemicals used in this study were of analytical grade (purity $\geq$99%) and used as received. All the solutions were prepared with Milli-Q water.

Instrumentation: The TEM images of the nanoparticles were obtained with FEI-TECNAI G2 205-TWIN electron microscope operating at 200 kV. The X-ray diffraction (XRD) analysis was performed with a Panalytical X'pert PRO high resolution XRD (PW 3040/60) unit using Ni-filtered Cu $K\alpha(\lambda = 1.54$ Å) radiation. The overall atomic percentage of the alloy catalyst was

measured with CAMECA sx-100 electron probe micro analyzer (EPMA). Electrochemical measurements were carried out in a two-compartment three-electrode cell using glassy carbon (GC) disk and a rotating ring-disk (RRDE Pt-GC, disk area: 0.196 cm², collection efficiency: 37 %) working (Pine, USA), Pt wire auxiliary, and Ag/AgCl (3 M KCl) reference electrodes. All electrochemical experiments were performed with Autolab potentiostat-galvanostat (302N), using computer controlled GPES software. All the potentials are referred against standard hydrogen electrode (SHE).

Synthesis of Pt-on-Pd dendritic nanostructures on MWCNTs: The Pt-on-Pd nanoparticles of different compositions were obtained by controlling the initial molar ratio of both precursors ($PtCl_6^{2-}$: $PdCl_4^{2-}$ = 2:1, 1:1, 1:4). In a typical synthesis of Pt-on-Pd bimetallic dendritic nanostructures, 3 mL of aqueous solution containing required concentration of $PtCl_6^{2-}$ and $PdCl_4^{2-}$ precursors were placed on a magnetic stirrer in a small beaker. Purified MWCNTs (2 mg) were added to the reaction mixture and stirred for 15 minutes. Then 15.84 mg of AA was rapidly added into the aqueous mixture under stirring. The final concentration of AA in the reaction mixture was 30 mM. The stirring was continued for 4 h for the complete reduction of both precursors. The molar ratio of metal precursors and AA in all the synthetic procedure was maintained at 1:30. The reaction mixture was filtered off and the catalyst was dried under vacuum at room temperature. The filtrate was colorless and it does not contain unreacted precursors, as evidenced from the absence of spectral signature, confirming the complete reduction of both the precursors. The Pt and Pd nanoparticles (nPt and nPd) were synthesized at an identical procedure using the corresponding precursors.

Electrode modification: The Pt-GC RRD electrodes were polished well with fine emery paper and alumina (0.05 µm) slurry and sonicated in Millipore water for 5-10 min to remove the

physically adsorbed impurities. These electrodes were washed repeatedly with sufficient amount of Milli-Q water and dried under argon atmosphere at room temperature. The catalyst ink was prepared by mixing the catalyst with 1% ethanolic Nafion[®] solution (2 mg/mL) and sonicated for 10 min. The cleaned electrodes were then modified with 10 µL of the resulting ink and dried in ambient condition for 30 min. All the electrocatalytic experiments were performed in 0.5 M H_2SO_4. The metal loading on the electrode was kept at ~25 µg/cm^2. In the case of Pt black, the metal loading was kept at rather high level (51.02 µg/cm^2) as lower loading is known to restrict the diffusion limiting current.[41] All the experiments were performed for at least three times and reproducible results were obtained.

Result and Discussion

Synthesis of Pt-on-Pd bimetallic electrocatalyst: Scheme 1 illustrates the probable growth mechanism involved in the synthesis of Pt-on-Pd nanodendrite over MWCNTs. In the synthesis of Pt-on-Pd nanostructures, the pale yellow color of the reaction mixture (MWCNTs, $PtCl_6^{2-}$ and $PdCl_4^{2-}$) turned to grey immediately after the addition of AA and then it became black while stirring for 4h at room temperature. In order to understand the mechanistic pathway for the co-reduction of Pt(IV) and Pd(II) precursors, the individual reduction of the precursors by AA was performed separately with 1:2 molar ratio (precursor:AA). The reduction potential of $PdCl_4^{2-}$/Pd (0.62 V) and $PtCl_6^{2-}$/Pt (0.725 V)[42] suggests that the reduction of Pt(IV) is highly facile compared to Pd(II). In the spectral measurement, the absorption band corresponding to $PdCl_4^{2-}$ at 235 nm disappeared immediately after the addition of AA and the solution turned initially to grey and then to brown in 30 min. On the other hand, the characteristic spectral band corresponding to $PtCl_6^{2-}$ at 262 nm disappeared and the solution became colorless only after 2 h stirring at room temperature. No characteristic feature for the formation of Pt nanoparticle was

observed. The change of color can be ascribed to the formation of $PtCl_4^{2-}$ species. Here the nanoparticle growth was noticed only after extensive stirring for long time (36 h) at room temperature (Figure 1). To further delve into the actual reaction pathway, time-dependent spectral measurement with $PtCl_6^{2-}$ and AA was performed at 1:2 molar ratio. In the time-dependent measurement, a new band at ~300 nm was observed at the expense of the characteristic band at ~262 nm after 24 h. The origin of the peak at 300 nm was investigated in detail to understand the mechanism involved in the reduction of $PtCl_6^{2-}$. It should be pointed out here that in aqueous solution AA behaves as a mild reducing agent. The oxidation of AA involves $2e^-$ and $1H^+$ in neutral pH and dehydroascorbic acid (DHA) is the oxidized product of AA. DHA is known to undergo hydrolysis in neutral or alkaline pH to produce 2, 3-diketogulonic acid.[43] However, DHA is highly stable in pH<5.[44] As the pH of our reaction mixture is <5, DHA is the only product from AA during the reaction. To verify the origin of the new band ~300 nm, spectral measurement was performed for the mixture of 1:1 molar ratio of $PtCl_4^{2-}$ and DHA. Interestingly, the spectrum obtained for the mixture shows a distinct band at ~300 nm (Figure 1d), which is very similar to that obtained during the reaction of AA and $PtCl_6^{2-}$ (Figure 1c). It is well established that the Pt(II) complex can undergo facile complexation with AA and DHA.[45-47] The new spectral band at 300 nm for the reaction mixture could be due to the $PtCl_4^{2-}$-DHA complex. Such complexation of Pt(II) with DHA can alter the reduction potential. In our synthesis of Pt-on-Pd nanodendrite, AA first reduces the Pd(II) precursor to Pd(0) and Pt(IV) to Pt(II). Pd(0) nucleates on the surface of MWCNT and yields surface-confined Pd nanoparticles. The Pt(II) species in solution undergo complexation with in-situ generated DHA before it finally reduced to Pt(0) by the excess AA present in the reaction mixture. The surface-confined Pd actually functions as a seed for the nucleation of Pt. The Pt atom nucleates over the

Pd seeds confined over MWCNTs and slowly grows further as a dendritic nanostructure (Figure S1).

It is well know that the Pd(0) and Pt precursors ($PtCl_6^{2-}$or $PtCl_4^{2-}$) can undergo spontaneous galvanic displacement reaction in aqueous solution.[26] Such reaction can be expected in our experimental condition as the reaction mixture initially contain Pd(0) and Pt(II) species. In order to verify the presence of such reaction, a control experiment with $PtCl_4^{2-}$ in the presence of DHA and Pd(0) was performed. Pd nanoparticles were synthesized separately and added to the mixture of $PtCl_4^{2-}$ and DHA and stirred for 2 days. The spectral measurement for the mixture at different time interval did not show any change in the spectral signature of $PtCl_4^{2-}$ (Figure S2), confirming that the in-situ generated Pt(II) complex in the presence of DHA does not undergo galvanic displacement reaction with the Pd nanoparticles. The absence of such reaction could be due to the complexation of Pt(II) with DHA.

Structural characterization of bimetallic catalyst: The overall atomic percentage of Pt and Pd in the bimetallic electrocatalyst was obtained by EPMA measurement from 10 different regions of the sample. Bimetallic electrocatalysts with varying Pt atomic ratio were analyzed and their composition was found to be $Pt_{64}Pd_{36}$, $Pt_{52}Pd_{48}$ and $Pt_{21}Pd_{79}$. The XRD pattern of MWCNT-supported $Pt_{64}Pd_{36}$ and $Pt_{21}Pd_{79}$ nanoparticles has characteristic pattern for face centered cubic (fcc) lattice (Figure S3). With the increasing the amount of Pd in the bimetallic electrocatalyst, the diffraction peaks were slightly shifted to higher angle, supporting the effective interaction between Pt and Pd in the bimetallic electrocatalyst. The calculation of lattice parameter (Table 1) shows that the bimetallic electrocatalyst has unit cell length in between the individual metals, possibly due to the fact that Pt and Pd have very similar fcc crystalline structure. Figure 2 represents the TEM images of MWCNT-supported bimetallic electrocatalysts of $Pt_{64}Pd_{36},$

$Pt_{52}Pd_{48}$ and $Pt_{21}Pd_{79}$ compositions. Dendritic growth of bimetallic nanoparticles over MWCNTs with an average size of 55 ($Pt_{64}Pd_{36}$) and 27 nm ($Pt_{52}Pd_{48}$) was observed; the branch width of the particles was found to be 2-5 nm (Figure 2). The HRTEM image of $Pt_{64}Pd_{36}$ composition shows the fringe spacing corresponding to the (100) plane. On the other hand, $Pt_{52}Pd_{48}$ and $Pt_{21}Pd_{79}$ composition has the fringe spacing corresponding to (111) plane. The shape and surface morphology of the $Pt_{21}Pd_{79}$ bimetallic nanostructure was completely different (Figure 2c). Although the growth of the anisotropic nanostructures over MWCNT was observed, growth of dendritic structure as in the case of other two compositions was not observed, presumably due to the presence of less amount of Pt precursor. It is considered that the dendritic Pt actually grows over the Pd nanoparticles on MWCNTs. The monometallic nPds on MWCNTs have an average size of 22 nm with a quasi-spherical and polyhedral shape (Figure S4). The average size of all bimetallic PtPd nanoparticles is larger than nPds. The nanoparticles obtained at an intermediate stage (30 min) during the synthesis of $Pt_{64}Pd_{36}$ composition have an average size of ~40 nm, which is larger than nPds but smaller than the bimetallic nanoparticles obtained after the completion of the reaction (Figure S1), suggesting that the growth of dendritic structure occurs over the nPds on MWCNTs. Moreover, EDS measurement for the nanoparticle obtained at 30 min shows the signature for Pt, supporting the growth of PtPd bimetallic nanoparticles (Figure S5). The mean crystallite size of the different electrocatalyst was calculated from the X-ray line broadening analysis and summarized in Table 1. It can be seen that the calculated size of $Pt_{21}Pd_{79}$ and nPd matches well with TEM measurement, whereas the calculated size of $Pt_{64}Pd_{36}$ and $Pt_{52}Pd_{48}$ as well as nPt does not match with the TEM measurements. It may be due to the fact that diffraction at dendritic surface does not meet the requirement for the use of Scherrer formula of a

crystalline surface. It is known that Scherrer constant ($k = 0.9$) is actually valid for spherical crystals with cubic symmetry.[48]

Electrochemical characterization: All the electrocatalysts were characterized by cyclic voltammetric measurement in 0.5 M H_2SO_4 under inert environment. The PtPd bimetallic electrocatalyst shows a well-defined voltammetric profile corresponding to the hydrogen adsorption/desorption as well as for the oxide formation and reduction (Figure S6). The electrochemically accessible surface area (ECSA) of all the electrocatalyst was estimated from the double layer corrected charge associated with the adsorption/desorption of under potential deposited hydrogen, assuming a value of 210 $\mu C/cm^2$ for the adsorption of a monolayer of hydrogen[49] and are summarized in Table 2.

Electrocatalytic reduction of oxygen: The electrocatalytic activity of the Pt-on-Pd bimetallic electrocatalyst towards ORR was tested in acidic electrolyte. Polarization curves for oxygen reduction were registered at different rotation rates with electrocatalyst-based rotating ring-disk electrode (Figure S7). The potential of the disk was scanned form 0.3 V to 1.2 V at a scan rate of 5 mV/s while holding the ring potential at 0.85 V for the detection of H_2O_2, if generated at the disk during ORR. Gradual increase in the limiting current was observed while increasing the rotation rates, indicating mass transfer controlled reduction of oxygen. No measurable current was detected at the ring confirming direct 4e⁻ reduction of oxygen on the electrocatalyst-based electrodes. Kinetic current density and other electrochemical parameters of ORR were calculated using the polarization curve at 1600 rpm with the help of following Koutecky-Levich equation.

$$\frac{1}{i} = \frac{1}{i_k} + \frac{1}{i_L} = \frac{1}{nFAkC} + \frac{1}{0.62nFAD^{2/3}\upsilon^{-1/2}C\omega^{1/2}}$$

where i_k is the kinetic current, representing the current in the absence of any mass transfer, i_L is the diffusion limiting current, F is the Faraday constant, C is the concentration of dissolved oxygen in dilute H_2SO_4 solution (1.1×10^{-6} mol/cm^3), n is the number electron transferred, A is the area of electrode/electrocatalyst, D is the diffusion coefficient of oxygen (1.9×10^{-5} cm^2/s), υ is the kinematic viscosity (1×10^{-2} cm^2/s) and ω is the electrode rotation rate. Electrocatalytic activity of the bimetallic electrocatalysts has been compared with the nPts synthesized in identical condition as well as with the commercial catalyst Pt balck (Figure 3). Electrochemical parameters of different electrocatalyst tested are summarized in Table 2. It was found that the specific and mass activity of $Pt_{64}Pd_{36}$ catalyst is significantly higher than all other catalysts tested. It is important to note that although Pt black exhibit more positive $E_{1/2}$ than the $Pt_{64}Pd_{36}$, the specific activity of the Pt black is ~7.5 times lower than that of bimetallic electrocatalyst. The $Pt_{64}Pd_{36}$ electrocatalyst show high specific activity with a metal loading of ~25 µg/cm^2, which is almost half compared to the Pt black (51.02 µg/cm^2). The mass specific activity of the $Pt_{64}Pd_{36}$ electrocatalyst is 2-3 times higher than that of other bimetallic electrocatalyst tested, and ~1.5 times higher when compared with nPt (Figure S8). Although the $Pt_{21}Pd_{79}$ catalyst has ~3 times lower Pt content than $Pt_{64}Pd_{36}$, it has relatively high specific activity with respect to the $Pt_{52}Pd_{48}$ catalyst (Table 2, Figure S9). The high specific activity of $Pt_{21}Pd_{79}$ may be ascribed to the maximum utilization of Pt.

The high specific activity of the $Pt_{64}Pd_{36}$ electrocatalyst can be justified by considering the structural and electronic effects. The adsorbed OH species on the catalyst surface is known to have energetic effect on the kinetics of ORR.[50] It is generally accepted that the adsorbed OH species can block the catalyst surface and decrease the ORR activity. The decreased formation of PtOH can significantly enhance the ORR activity. The surface morphology and structure of the

catalyst may contribute to the decreased formation of such species. The close examination of the voltammetric profile obtained for the nanoelectrocatalysts of different compositions in H_2SO_4 solution (Figure S6) shows that the formation of PtOH decreases in the order of $Pt_{52}Pd_{48}$ >$Pt_{21}Pd_{79}$>$Pt_{64}Pd_{36}$, probably due to the difference in the crystallographic orientation and surface morphology. The oxide formation on $Pt_{64}Pd_{36}$ occurs at slightly more positive potential with respect to the others. Such decreased formation of PtOH is partially responsible for the enhanced activity of $Pt_{64}Pd_{36}$. As shown in Figure 3B and Table 2, the area specific and mass specific activity of the nanoelectrocatalysts increases in the order of $Pt_{52}Pd_{48}$ <$Pt_{21}Pd_{79}$ <$Pt_{64}Pd_{36}$. It is considered that the change in the electronic state of the alloy electrocatalyst is one of the main reasons behind the enhanced ORR activity of $Pt_{64}Pd_3$. The Pd-induced compressive strain can decrease the binding of OH and hence an enhancement in the catalytic activity of the catalyst. The presence of Pd subsurface beneath the Pt dendrites actually induces an ideal d-band vacancy. As discussed earlier, the downshift of the d-band center of PdPt core-shell nanostructure considerably enhances the ORR activity.[20] A downshift of the d-band center with respect to the Fermi level would weaken the interaction between the reactive catalyst surface and adsorbed OH and essentially lowers the M-O/OH bond energy. Furthermore, the HRTEM image of $Pt_{64}Pd_3$ reveal the presence of (100) planes in the branches of the nanodendrites. It is well established that the (100) planes are more reactive towards oxygen reduction in H_2SO_4 solution compared to (111) planes.[52] The combined structural and electronic effects actually contribute to the enhanced activity of the $Pt_{64}Pd_{36}$ with respect to the other nanoparticles. The increased formation of PtOH and the presence of (111) crystallographic orientation can be accounted for less reactivity of $Pt_{52}Pd_{48}$ and $Pt_{21}Pd_{79}$ nanoparticles. The present investigation with different compositions of Pt and Pd essentially solicits for the ideal bimetallic composition for enhanced ORR activity.

Durability test: Durability of all the electrocatalyst was evaluated by cycling the potential between 0.6 V to 1.2 V in oxygen saturated 0.5 M H_2SO_4 solution. After 1000 potential cycles, the ECSA and ORR activity were measured. The bimetallic catalyst with $Pt_{64}Pd_{36}$ composition was found to have high durability with almost no change in the catalytic current density indicating the excellent durability (Figure 4). A loss of ~7.5% ECSA was observed for $Pt_{64}Pd_{36}$ catalyst after extensive cycle (Figure S10). In the case of $Pt_{52}Pd_{48}$ composition, though the half-wave potential remained almost same (only 2 mV negative shift), considerable decrease in the catalytic current density was observed. On the other hand, the $Pt_{21}Pd_{79}$ and nPts have poor durability; the possible dissolution of the Pd atoms during extended cycling in the acidic environment[53] can be accounted for the lack of durability of the $Pt_{21}Pd_{79}$ catalyst (Figure S11). The voltammetric experiments performed for ORR with nPds show that the nanoparticles are not durable (Figure S12). Significant decrease in the peak current and negative shift in the peak potential were noticed during potential cycling, presumably due to the dissolution of nPds from MWCNTs. A significant decrease in the catalytic activity was found in the case of $Pt_{21}Pd_{79}$ and Pt catalyst with a negative shift of 18-20 mV (Figure S10) in the half wave potential. Thus it is understood that the electrocatalytic activity and durability of the bimetallic catalyst can be manipulated by varying the atomic ratio of the individual metal.

Summary

The dendritic Pt-on-Pd bimetallic nanostructures of different compositions were grown over MWCNTs in the absence of surfactants and their electrocatalytic activity towards ORR has been examined. The Pd(II) complex first reduced to Pd(0) and confine on the walls of MWCNTs. The Pt atoms then nucleate over the surface-confined Pd nanoparticles. It is demonstrated for the first time that the reduction of Pt(IV) to Pt(0) by AA involves the formation

of Pt(II)-DHA complex. Electrocatalytic performances of the bimetallic electrocatalyst were compared in terms of kinetic current density, mass activity and durability. The $Pt_{64}Pd_{36}$ has high electrocatalytic activity and durability. The structural and electronic effects contribute for the enhanced activity of the $Pt_{64}Pd_{36}$ catalyst. It is hypothesized that underlayer Pd atoms strongly influence the catalytic activity of the dendritic surface. This study reveals the advantage of decoration of MWCNTs with bimetallic nanostructures of enhanced durability and electrocatalytic activity.

Acknowledgement

References

[1]   E. Yeager, *Electrochim. Acta* 1984, **29**, 1527.

[2]   A. B. Anderson, J. Roques, S.Mukerjee, S. Murthi, *J. Phys. Chem. B* 2005, **109**, 1198.

[3]   S. L. Chen, A. Kucernak, *J. Phys. Chem. B* 2004, **108**, 3262.

[4]   J. O'M. Bockries, A. K. N. Reddy, In *Modern electrochemistry*, Plenum press, New York, **1970**, vol 2.

[5]   V. Jalan, E. J. Taylor, *J. Electrochem. Soc*. 1983, **130**, 2299.

[6]   B. C.Beard, P.N Ross, *J. Electrochem. Soc*. 1990, **137**, 3368.

[7]   M. T. Paffet, G. J. Beery, S. Gottesfeld, *J. Electrochem. Soc.* 1988, **135**, 1431.

[8]   S. Mukerjee, S. Srinvasan, M.P. Soriaga, *J. Electrochem. Soc.* 1995, **142**, 1409.

[9]   M. K. Min, J.H. Cho, K. W. Cho, H. Kim, *Electrochim. Acta* 2000, **45**, 4211.

[10]   M. Watanabe, K. Tsurumi, T. Mizukami, T. Nakamura, P.Stonehart, *J. Electrochem. Soc*. 1994, **141**, 2659.

[11]   Z. Sun, C. C. A. Tseung, *Electrochem. Solid State Lett.* 2000, **3**, 413.

[12]   A. J. Appleby, *Catal. Rev.* 1970, **4**, 221.

[13]   B. Hammer, J. K.Nørskov, *Surf. Sci.* 1995, **343**, 211.

[14]   J. R. Kitchin, J. K.Nørskov, M. A.Barteau, G.Chen, *J. Chem.Phys.* 2004, **120**, 10240.

[15]   B. Hammer, J.K. Nørskov, *Adv. Catal.* 2000, **45**, 71.

[16]   J. Greeley, J. K. Nørskov, M. Mavrikakis, *Ann. Rev. Phys. Chem.* 2002, **53**, 319.

[17]   M. Shao, P. Liu, J.Zhang, R. R.Adzic, *J. Phys. Chem. B* 2007, **111**, 6772.

[18]   W. P. Zhou, X. Yang, M. B.Vukmirovic, B. E.Koel, J. Jiao, G. Peng, M. Mavrikakis, R. R.Adzic, *J. Am. Chem. Soc*. 2009, **131**, 12755.

[19]   P. Strasser, S. Koh, T. Anniyev, J. Greeley, K. More, C. Yu, Z. Liu, S. Kaya, D. Nordlund, H. Ogasawara, M. F.Toney, A.Nilsson, *Nature Chem*. 2010, **2**, 454.

[20]   C. Koenigsmann, A. C.Santulli, K.Gong, M. B.Vukmirovic, W. P.Zhou, E.Sutter, S. S. Wong, R. R. Adzic, *J. Am. Chem. Soc*. 2011, **133**, 9783.

[21]   W. He, J. Liu, Y. Qiao, Z. Zou, X. Zhang, D.L. Akins, H. Yang, *J. Power Sources* 2010, **195**, 1046.

[22]   Y. Li, Z.W. Wang, C.Y. Chiu, L.Ruan, W. Yang, Y. Yang, R.E. Palmer, Y. Huang, *Nanoscale* 2012, **4**, 845.

[23]   Z. Peng, H. Yang, *J. Am. Chem. Soc*. 2009, **131**, 7542.

[24]   H. Zhang, M. Jin, J. Wang, W. Li, P.H. Camargo, M.J. Kim, D. Yang, Z.Xie, Y. Xia, *J. Am. Chem. Soc.* 2011, **133**, 6078.

[25]   S. Ghosh, R. K. Sahu, C.R. Raj, *Nanotechnology* 2012, **23**, 385602.

[26]   D. Wang, H.L.Xin, Y. Yu, H. Wang, E.Rus, D.A. Muller, H.D.Abruña, *J. Am. Chem. Soc.* 2010, **132**, 17664.

[27]   J. Chen, T. Herricks, Y. Xia, *Angew. Chem. Int. Ed.*2005, 44, 2589.

[28]   Y.W. Lee, N.H. Kim, K.Y. Lee, K. Kwon, M. Kim, S.W. Han, *J. Phys. Chem. C* 2008, **112**, 6717.

[29]   H. Kochkar, M.Aouine, A.Ghorbel, G.Berhault,*J. Phys. Chem. C* 2011, **115**, 11364.

[30]   H. Wang, H.Y.Jeong, M.Imura, L. Wang, L.Radhakrishnan, N. Fujita, T. Castle, O.Terasaki, Y. Yamauchi, *J. Am. Chem. Soc.* 2011, **133**, 14526.

[31]   L.Wang, Y.Nemoto, Y. Yamauchi, *J. Am. Chem. Soc.* 2011, **133**, 9674.

[32]   L. Wang, Y. Yamauchi, *Chem. Mater.* 2009, **21**, 3562.

[33]   H. Zhang, Y. Yin , Y. Hu , C. Li, P. Wu , S. Wei, C. Cai, *J. Phys. Chem. C* **2010**, *114*, 11861.

[34]   H.Lee, S. Habas, G.A. Somorjai, P. Yang, *J. Am. Chem. Soc.* 2008, **130**, 5406.

[35]   B. Lim, M. Jiang, T. Yu, P.H. Camargo, Y. Xia. *Nano Res.* 2010, **3**, 69.

[36]   B. Lim, M. Jiang, P.H. Camergo, E.C. Cho, J. Tao, X. Lu, Y. Zhu, Y. Xia, *Science* 2009, **324**, 1302.

[37]   S. Ghosh, C.R. Raj, *J. Phys. Chem. C.* 2010, **114***,* 10843.

[38]   B.K. Jena, C. R. Raj, *J. Phys. Chem. C* 2008, **112**, 3496.

[39]   S. Chakraborty, C.R. Raj, *Carbon* 2010, **48**, 3242.

[40]   S. Ghosh, C.R. Raj, *Catal. Sci. Technol.,* 2013, **3**, 1078.

[41]   K. J.J. Mayrhofer, D. Strmcnik, B.B. Blizanac, V. Stamenkovic, M. Arenz, N.M. Markovic, *Electrochim. Acta* 2008, **53**, 3181.

[42]   T. Nakamura, S. Ichihara, T. Den, *ECS Trans*. 2007, **3**, 275.

[43]   Y. Nishikawa, T.Kurata, *Biosci. Biotechnol.Biochem*. 2000, **64**, 476.

[44]   I. Koshiishi, Y. Mamura, T. Imanari, *Biochim. Biophys.Acta* 1998, **1379**, 257.

[45]   P. Bergamini, E.Marchesi, V.Bertolasi, M.Fogagnolo, L.Scarpantonio, S.Manfredini, S. Vertuani, A. Canella, *Eur. J. Inorg. Chem.* 2008, 529.

[46]   R. N. Bose, E.L. Weaver, *J. Chem. Soc., Dalton Trans.*, 1997, 1797.

[47]   E. L. Weaver, R.N. Bose, *J. Inorg. Biochem.* 2003, **95**, 231.

[48]   B. D. Cullity, in *Elements of X-ray Diffraction*, Addison-Wesley Publishing Company Inc., USA 1956, Ch. 6.

[49]   S. Trasatti, A.Petrii, *Pure Appl. Chem*. 1991, ***63***, 711.

[50]   J. Zhnag, Y. Mo, M.B. Vukmirovic, R. klie, K. Sasaki, R.R. Adzic, *J. Phys. Chem. B* 2004, ***108***, 10955.

[51]   X. Dang, A. M. Massari, J. T. Hupp, *Electrochem. Solid-State Lett*. 2000, *3*, 555.

[52]   N. M. Markovic, H.A.Gasteiger, P.N. Ross, P. N. *J. Phys. Chem*. 1995, ***99***, 3411.

[53]   J. P. Hoare, *J. Electrochem. Soc.* 1964, **111**, 610.

Scheme 1

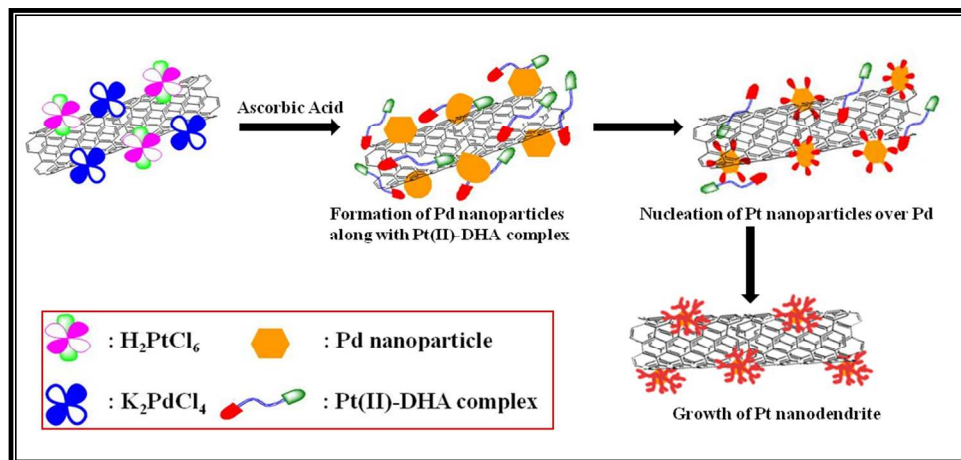Probable mechanism for the growth of Pt-on-Pd dendritic nanostructures over MWCNT.

Figure 1

The UV-vis spectral profile illustrating the formation of Pt(II)-DHA complex during the reduction of H_2PtCl_6 by AA. (a) $PtCl_6^{2-}$, (b) mixture of $PtCl_6^{2-}$ and AA, (c) mixture of $PtCl_6^{2-}$ and AA after 24 h, (d) $PtCl_4^{2-}$ and DHA after 24 h and (e) DHA.
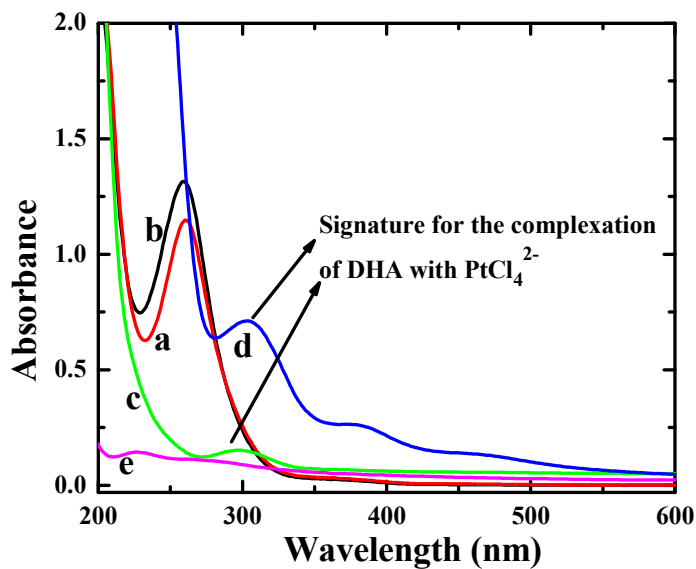
Figure 2

TEM images of MWCNT-supported (a) $Pt_{64}Pd_{36}$ (b) $Pt_{52}Pd_{48}$ and (c) $Pt_{21}Pd_{79}$ nanoelectrocatalysts. Inset shows the HRTEM image.
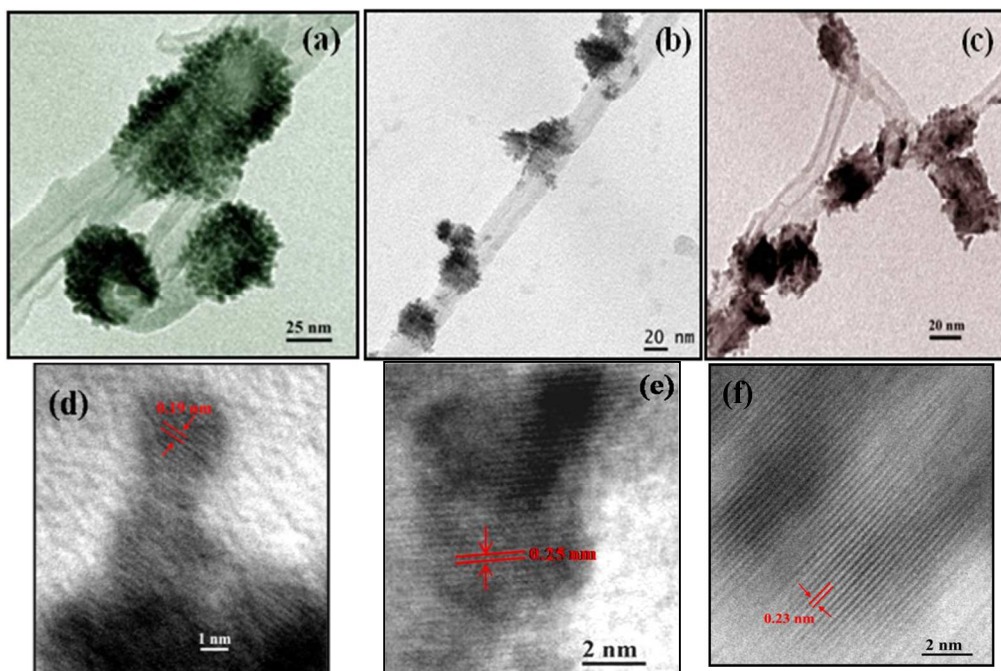
Figure 3

(A) Polarization curve obtained for ORR with (a) $Pt_{64}Pd_{36}$, (b) nPt and (c) Pt-black in 0.5 M H_2SO_4. Rotation rate: 1600 rpm. Scan rate: 5 mV/s. Ring potential: 0.85 V. Current is normalized with the electrochemically active surface area. (B) Plot depicting the mass specific activity of the electrocatalysts.
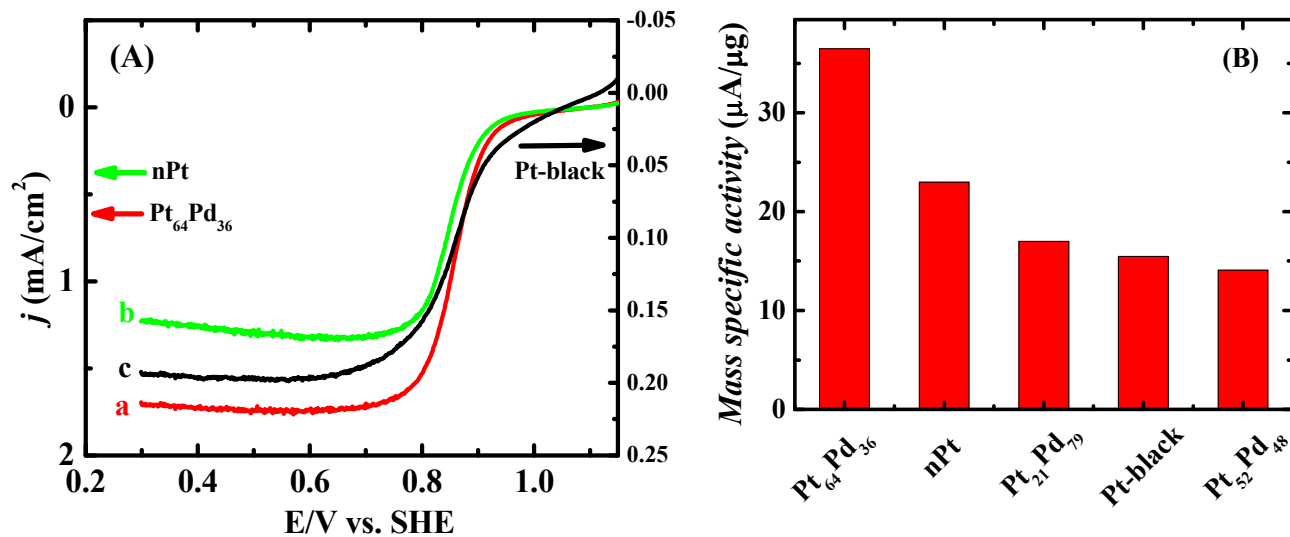
Figure 4

Polarization curve illustrating the durability of $Pt_{64}Pd_{36}$/MWCNT electrocatalyst. The electrode modified with the catalyst was subjected to 1000 potential sweeps. Rotation rate: 800 rpm. Other experimental conditions are the same as in figure 3.
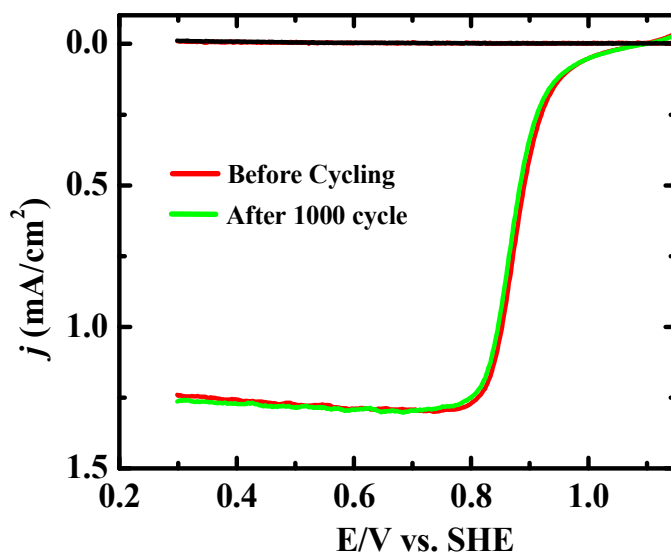
Table 1

Particle size and lattice parameter for the MWCNT-supported mono and bimetallic electrocatalysts.

Catalyst	Particle size d (nm)		Lattice parameter, a (Å)
	XRD	**TEM***	
Only Pt	15.12	45	3.905
Pt$_{64}$Pd$_{36}$	13.02	55	3.903
Pt$_{52}$Pd$_{48}$	10.79	27	3.898
Pt$_{21}$Pd$_{79}$	22.32	25	3.896
nPd	24.88	22	3.894

* Average size

Table 2

Electrocatalytic performance of the nanoelectrocatalysts towards ORR. Polarization curve obtained at 1600 rpm were used to analyze the ORR activity.

Catalyst	ECSA (cm^2)	Onset* Pot. (V)	j_k (mA/cm^2)**	Mass activity $(\mu A/\mu g)$**
$Pt_{21}Pd_{79}$	0.63	1.011	0.150	17
$Pt_{52}Pd_{48}$	0.54	1.012	0.130	14
$Pt_{64}Pd_{36}$	0.58	1.062	0.342	36.5
nPt	0.65	1.066	0.214	23
Pt Black	3.22	1.09	0.046	15.1

* *It is the intersection point of the two tangents drawn to the linear part of the curve.*[51]

** Calculated at 0.9 V. Current is normalized with ECSA.